JOURNAL OF MAGNETIC RESONANCE **126,** 48–57 (1997)
ARTICLE NO. MN971131

NMR Relaxation Mechanisms for Backbone Carbonyl Carbons in a ^{13}C, ^{15}N-Labeled Protein

Peter Allard* and Torleif Härd

Center for Structural Biochemistry, Royal Institute of Technology, Novum, S-141 57 Huddinge, Sweden

Received September 23, 1996; revised January 15, 1997

The predominant relaxation mechanisms for backbone carbonyl carbon ($^{13}C'$) relaxation in a ^{13}C, ^{15}N-doubly enriched sample of the thermostable Sso7d protein have been investigated. Pulse sequences for measurements of longitudinal and transverse $^{13}C'$ relaxation rates were implemented, and these rates were measured at magnetic fields of 11.7 and 14.1 T. The field dependence in measured rates is small and consistent with a predominant contribution from chemical-shift anisotropy (CSA) to $^{13}C'$ relaxation. A pulse sequence for measurement of $\{^1H\}-^{13}C'$ cross-relaxation rates (steady-state NOEs) was also developed. This experiment reveals a significant NOE between protons and all $^{13}C'$, indicating that dipolar interactions between these nuclei contribute to $^{13}C'$ relaxation. Experiments designed to suppress cross correlation between CSA relaxation and dipole–dipole (DD) relaxation due to neighboring $^{13}C^{\alpha}$ indicate that this effect is negligible. A more quantitative treatment is also presented, in which backbone dynamics parameters are fitted to average $^{13}C'$ relaxation rates using Lipari–Szabo expressions for the spectral density. This fit, which reproduces well expected backbone dynamics parameters for a folded protein, is used to estimate the relative contributions of various mechanisms to $^{13}C'$ relaxation. It is found that both longitudinal and transverse relaxation rates are dominated by CSA relaxation and contain significant contributions due to DD relaxation induced by nearby protons. Contributions from DD relaxation due to covalently bound $^{13}C^{\alpha}$ and ^{15}N are comparably small. The predominant effects of CSA and $^1H-^{13}C'$ DD interactions, for which physical and geometrical parameters are uncertain, complicate the use of $^{13}C'$ relaxation as a sequence-specific probe for protein backbone dynamics.

INTRODUCTION

NMR relaxation of different nuclei is frequently used to study dynamics in proteins and other molecules. This is possible since the relaxation rates depend on motions of vectors in the molecule (*1*). The relaxation rates also depend on the type of relaxation mechanism involved and on the corresponding physical and geometrical parameters (*1*), and these need to be determined if NMR relaxation is to be used in studies of dynamics.

In principle, the relaxation of any proton (^1H), carbon (^{13}C), or nitrogen (^{15}N) spin in a protein will contain information about dynamics. The most common application is the use of ^{15}N relaxation measurements to characterize the dynamics in the polypeptide backbone (*2–4*) as well as that of certain amino acid side chains [e.g., arginine (*5*)]. The success of ^{15}N relaxation methods to study protein motions relies on the fact that the relaxation pathways of this nucleus in backbone amides are relatively well characterized and that ^{15}N enrichment in most cases is easily carried out. More recently also α-carbon ($^{13}C^{\alpha}$) relaxation has been used to extract information about backbone motions (*6, 7*). Additional complications associated with this nucleus, compared to backbone ^{15}N, are the poor resolution for $^{13}C^{\alpha}$ in a $^1H-^{13}C$ HSQC spectrum and poor sensitivity (for ^{13}C at natural abundance) or homonuclear J couplings that affect transverse relaxation rates (in the case of ^{13}C-enriched samples).

Here, we investigate the predominant relaxation mechanisms for backbone carbonyl carbon ($^{13}C'$) magnetization in a ^{13}C, ^{15}N-enriched protein. The investigation was motivated by the need to characterize backbone motions in a protein in which many of the amide protons exchange rapidly with the solvent under relevant pH conditions (*8*). In this case, the $^{13}C'$ magnetization would have been excited and detected via the α protons. However, in order to evaluate the relaxation pathways for $^{13}C'$ in proteins and the use of these rates for characterization of dynamics in ^{13}C, ^{15}N-enriched proteins, we have performed the measurements reported here on a protein that is better behaved in terms of availability, stability, and spectral resolution. The 7 kDa DNA-binding protein Sso7d is very stable and shows well-resolved NMR spectra, and the structure is known (*9*).

The application of $^{13}C'$ relaxation measurements in studies of protein dynamics was first reported by Dayie and Wagner (*10*), who measured longitudinal and transverse relaxation rates of all $^{13}C'$ in villin 14T at a single magnetic field. In that study, the effect of cross correlation (see below) was not considered, and no attempt was made to fit any

* To whom correspondence should be addressed.

1090-7807/97 $25.00

dynamic model. The heteronuclear cross-relaxation rate between $^{13}C^{\alpha}$ and $^{13}C'$ has also been suggested as a probe for backbone dynamics (*11, 12*). However, these two studies which are based on steady-state (*12*) and transient (*11*) NOE measurements do not completely agree on the magnitude of the order parameter for motions of the $^{13}C^{\alpha}-{}^{13}C'$ bond vector.

We have measured the longitudinal and the transverse relaxation rates for all backbone $^{13}C'$ in ^{13}C, ^{15}N-enriched Sso7d at two magnetic fields (11.7 and 14.1 T). The steady-state $\{^1H\}-{}^{13}C'$ NOE was measured to estimate the role of neighboring protons on $^{13}C'$ relaxation. Pulse sequences that suppress cross correlation (*13, 14*) between the dipole–dipole (DD), and the chemical-shift anisotropy (CSA) relaxation mechanisms have also been evaluated. These experimental data give direct indications about the contributions of CSA, DD auto-relaxation and $^1H-{}^{13}C'$ cross-relaxation mechanisms, as well as cross correlation between $^{13}C'$ CSA and $^{13}C'-{}^{13}C^{\alpha}$ DD interactions. A more quantitative treatment in which dynamic parameters are fitted to average observed rates using the Lipari–Szabo (*15, 16*) formalism is also presented. This fit, which yields very reasonable values for the backbone dynamics, is used to estimate the relative contributions of various mechanisms for $^{13}C'$ relaxation in doubly labeled proteins.

THEORY

Relaxation

The two most important mechanisms for $^{13}C'$ relaxation in proteins that are enriched in both ^{15}N and ^{13}C are DD relaxation and CSA relaxation. The rates for longitudinal and transverse DD relaxation of the spin S caused by the unlike spin I are (1)

$$R_1^{DD} = \frac{1}{4}\left(\frac{\mu_0}{4\pi}\right)^2 \hbar^2\gamma_I^2\gamma_S^2\frac{1}{\mathbf{r}_{IS}^6} \times [J(\omega_I-\omega_S)+3J(\omega_S)+6J(\omega_I+\omega_S)] \quad [1]$$

$$R_2^{DD} = \frac{1}{8}\left(\frac{\mu_0}{4\pi}\right)^2 \hbar^2\gamma_I^2\gamma_S^2\frac{1}{\mathbf{r}_{IS}^6} \times [4J(0)+J(\omega_I-\omega_S)+3J(\omega_S)+6J(\omega_I)+6J(\omega_I+\omega_S)], \quad [2]$$

where μ_0 is the permeability of vacuum, $\hbar$ is Plank's constant divided by 2π, γ_S and γ_I are the magnetogyric ratios of spin S and I, respectively, and $\mathbf{r}_{IS}$ is the distance between spin I and S. The angular Larmor frequencies of spins I and S are labeled ω_I and ω_S, respectively.

The corresponding rates for CSA relaxation of spin S are (*1*)

$$R_1^{CSA} = \frac{3}{4}\delta_{Z'}^2\left(1+\frac{\eta^2}{3}\right)\gamma_S^2B_0^2[J(\omega_S)] \quad [3]$$

$$R_2^{CSA} = \frac{1}{8}\delta_{Z'}^2\left(1+\frac{\eta^2}{3}\right)\gamma_S^2B_0^2[4J(0)+3J(\omega_S)], \quad [4]$$

where $\delta_{Z'}$ is the largest traceless principal component of the chemical-shift tensor and η is a parameter describing the asymmetry of the tensor. B_0 is the static magnetic field of the NMR magnet.

The heteronuclear cross-relaxation rate can be measured directly using transient methods or indirectly using the steady-state NOE and the total longitudinal relaxation rate. The equation for the heteronuclear cross-relaxation rate, σ_{IS}, is

$$\sigma_{IS} = \frac{1}{4}\left(\frac{\mu_0}{4\pi}\right)^2\hbar^2\gamma_I^2\gamma_S^2\frac{1}{\mathbf{r}_{IS}^6} \times [6J(\omega_I+\omega_S)-J(\omega_I-\omega_S)]. \quad [5]$$

The steady-state NOE is related to the heteronuclear cross-relaxation rate and the total longitudinal relaxation rate for spin S as

$$\text{NOE} \equiv \frac{I_{SAT}}{I_0} = 1+\frac{\gamma_I}{\gamma_S}\frac{\sigma_{IS}}{R_1^{tot.}}, \quad [6]$$

where I_{SAT} and I_0 are the intensities of a heteronucleus resonance spin S with and without saturation of the dipole–dipole connected neighbor, spin I.

CSA and DD relaxation have the same symmetry, and cross terms connecting the two relaxation mechanisms therefore appear in the Redfield relaxation matrix (*13, 14*). These interference or cross-correlation terms will redistribute elements of the density matrix during a time delay, but they will not restore them to equilibrium. Assuming an axially symmetric CSA tensor, this matrix element is, for longitudinal magnetization (*17*),

$$R_{CSA-DD} = -\left(\frac{\mu_0}{4\pi}\right)\hbar\gamma_S^2\gamma_I\frac{1}{\mathbf{r}_{IS}^3}(\sigma_\parallel-\sigma_\perp) \times B_0\frac{1}{2}[3\cos^2(\varphi)-1][J(\omega_S)], \quad [7]$$

where $\sigma_\parallel$ and $\sigma_\perp$ are the chemical shifts of the parallel and the perpendicular directions of the direction-dependent chemical-shift tensor, respectively, and φ is the angle be-

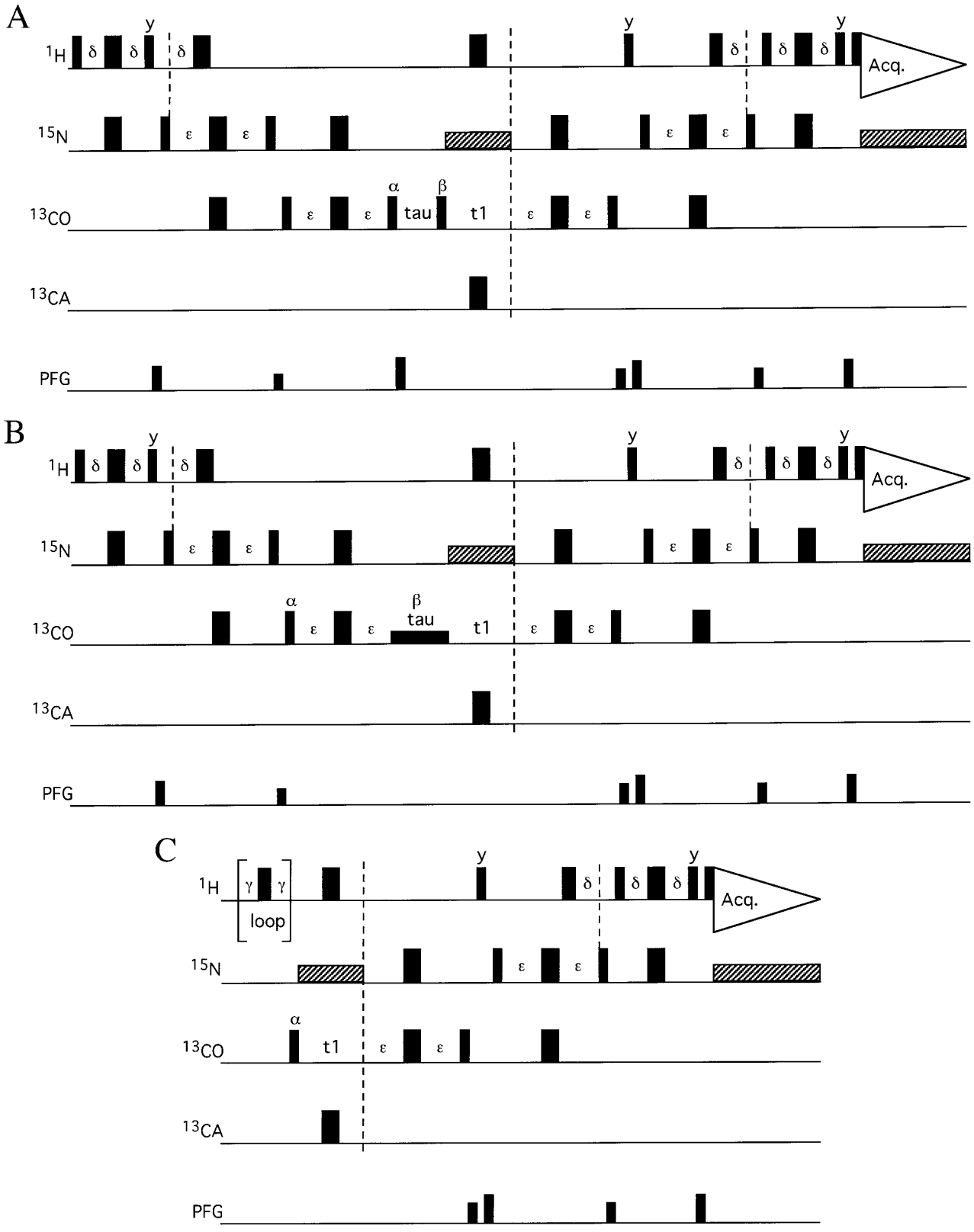

FIG. 1. Pulse sequences used for (A) the measurement of $^{13}C'$ longitudinal relaxation rates, (B) $^{13}C'$ transverse relaxation rates, and (C) the steady-state NOE between ^{1}H and $^{13}C'$. All phases are *x* unless otherwise indicated. Thin and thick vertical bars indicate 90° and 180° flip angles, respectively. To achieve selectivity between $^{13}C^{\alpha}$ and $^{13}C'$, all carbon pulses were set to 64 and 54 μs pulse lengths at 11.7 and 14.1 T, respectively. The tip angle

tween the unique axis of the CSA tensor and the internuclear vector $\mathbf{r}_{IS}$.

Dynamic Model

The dynamic model considered in this paper is that derived using the Lipari–Szabo approach (*15, 16*). The analytical spectral density function for this model is

$$J(\omega) = \frac{2}{5}\left[\frac{S^2\tau_m}{1 + (\omega\tau_m)^2} + \frac{(1 - S^2)\tau_i}{1 + (\omega\tau_i)^2}\right] \quad [8]$$

with

$$\frac{1}{\tau_i} = \frac{1}{\tau_m} + \frac{1}{\tau_e}, \quad [9]$$

where τ_m is the rotational correlation time, τ_e is the internal correlation time and, S^2 is the generalized order parameter that describes the balance between contributions to $J(\omega)$ due to overall rotation and internal motion. The Lipari–Szabo model is based on the assumption that the overall rotation is isotropic and that the two motions are statistically independent.

MATERIALS AND METHODS

Sample Preparation

An NMR sample containing ^{13}C, ^{15}N-labeled Sso7d (*9, 18*) was obtained from Dr. H. Baumann (now at Pharmacia & Upjohn) who produced the protein using an overexpression system and purification protocol kindly provided by S. Knapp and Professor R. Ladenstein (Karolinska Institute) (*19*). The NMR sample contained approx. 0.9 m*M* protein in 10 m*M* phosphates and 50 m*M* NaCl at pH 5.0.

NMR Relaxation Pulse Sequences

Pulse sequences for measurement of $^{13}C'$ longitudinal and transverse relaxation rates are presented in Figs. 1A and 1B. Both sequences start with a refocused INEPT (*20*) transfer of magnetization from the NH proton to the ^{15}N, directly followed by an overlapping second refocused INEPT transfer from ^{15}N to $^{13}C'$. At this point the in-phase $^{13}C'$ magnetization is either spin locked in a $R_{1\rho}$(R_2) experiment or placed along the z axis in an R_1 experiment. After a variable relaxation delay, the spin lock is released in the case of the $R_{1\rho}$ experiment or the magnetization is put back to the x–y plane in the case of the R_1 experiment. The magnetization is now frequency labeled with the $^{13}C'$ chemical shift before being transferred back to the NH proton for detection, using two more overlapping refocused INEPT transfers. The last two ^1H pulses and the final pulsed field gradient are not necessary but improve the water suppression (*21*). All carbon pulses were equally long, 64 μs at 11.7 T and 54 μs at 14 T, which for both 90° and 180° pulses corresponds to an excitation null close to the $^{13}C^\alpha$ region for $^{13}C'$ pulses, and vice versa. The tip angle was changed by adjusting the power level. All $^{13}C^\alpha$ pulses were doubly frequency shifted using phase modulation to +/− the $^{13}C^\alpha$ offset frequency (*22*) in order to eliminate nonresonant shifts on the $^{13}C'$ magnetization (*23*). Pulsed field gradients were applied to suppress the water resonance and to remove unwanted magnetization whenever the magnetization of interest was in the form of longitudinal magnetization or longitudinal two-spin order coherence (*24*). A proton 90°_y pulse was sandwiched between two pulsed field gradients when the magnetization was in the form of longitudinal two-spin order between $^{13}C'$ and ^{15}N in order to improve the water suppression. A minimal two-step phase cycle was used for the selection of $^{13}C'$ magnetization. In the R_1 experiment, the magnetization was alternately put along the positive and negative z axis during the relaxation delay time. This ensures that the relaxation rate does not depend on the equilibrium value of longitudinal magnetization and that the magnetization relaxes to zero as required for a two-parameter exponential fit (*25, 26*).

An R_2 sequence identical to the $R_{1\rho}$ sequence in which the continuous-wave field was replaced by a CPMG pulse train, with or without four $^{13}C^\alpha$ 180° pulses, was also used. The $^{13}C^\alpha$ pulses were applied at the following time points during the relaxation delay in order to suppress cross correlation between CSA and DD relaxation: delay/8—pulse—delay/4—pulse—delay/4—pulse—delay/4—pulse—delay/8. The same sequence of $^{13}C^\alpha$ pulses was applied to suppress cross correlation in some R_1 measurements.

The pulse sequence for measurement of steady-state NOE

---

was changed by changing the power level. The $^{13}C^\alpha$ decoupling pulses in the middle of the t_1 period was doubly frequency shifted using phase modulation of +/− the $^{13}C^\alpha$ offset frequency (*22*). Pulsed-field gradients were applied in order to suppress the water resonance and remove unwanted magnetization (*24*). States–TPPI was used for phase-sensitive detection during the t_1 period (*27*). In the longitudinal-relaxation-rate-measurement experiment (A), the magnetization was alternately put along the positive and negative z axis during the relaxation delay (*25, 26*). The spin-lock field strength in the transverse-relaxation-rate-measurement experiment (B) was set to 3.0 and 3.4 kHz at 11.7 and 14.1 T, respectively. The steady-state NOE-measurement pulse sequence (C) starts either with saturation of all ^1H using a train of 120° pulses with 5 ms delays between pulses during 5 s or with a equally long time delay without pulses. The delays used in all pulse sequences are as follows: δ = 2.72 ms and ϵ = 16.7 ms. The pulsed-field gradients were 2 ms long and applied with a strength in the range of ±2–20 G/cm. The phase cycling is employed as follows: (A) $\alpha = (y, -y)$; $\beta = y$; rec. = $(x, -x)$. (B) $\alpha = (x, -x)$; $\beta = y$; rec. = $(x, -x)$. (C) $\alpha = (y, -y)$; rec. = $(x, -x)$.

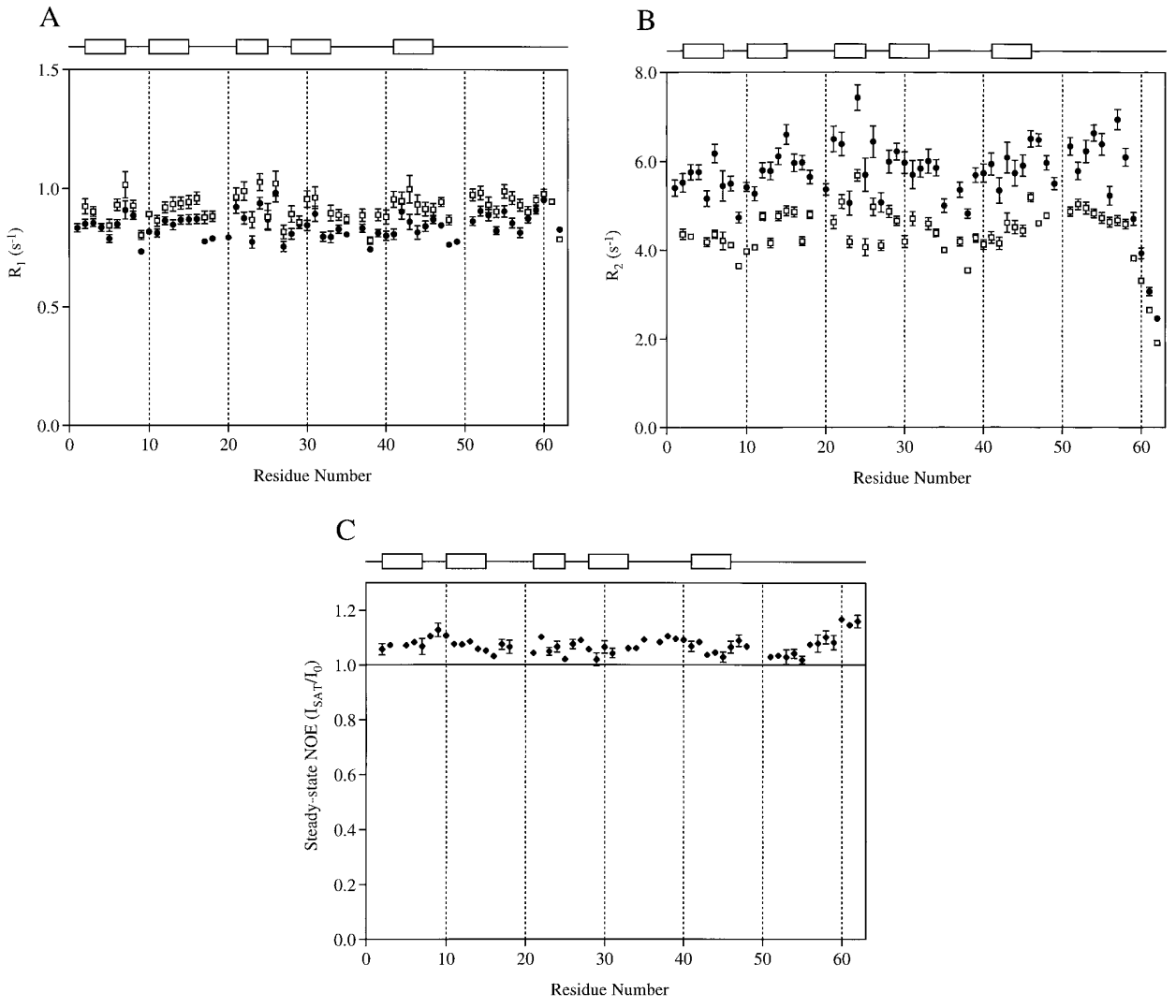

FIG. 2. $^{13}C'$ relaxation rates as a function of residue number for the DNA-binding thermostable protein Sso7d. Longitudinal relaxation rates (A) at 11.7 T (open squares) and 14.1 T (filled circles). Transverse relaxation rates (B) at 11.7 T (open squares) and 14.1 T (filled circles). Heteronuclear steady-state NOE (C) between ^1H and $^{13}C'$. Error bars are only plotted when larger than the plot symbol. The boxes above the figures indicate β sheets present in the structure (*9*).

is presented in Fig. 1C. The sequence starts either with saturation of ^1H using a train of pulses applied during a certain time or with an equally long time delay without pulses. The intensity of a resonance recorded with and without saturation is compared in the determination of the steady-state NOE. After this pulse train or delay, the $^{13}C'$ magnetization is placed in the *xy* plane, frequency labeled during t_1, and transferred to the NH proton for detection as in the longitudinal-relaxation-rate measurement pulse sequence in Fig. 1A.

NMR Relaxation Measurements

The longitudinal- and transverse-relaxation-rate experiments at 11.7 T were carried out with spectral widths of 6000 and 1500 Hz in ^1H and $^{13}C'$ dimensions, respectively. The $^{13}C'$ frequency was set to 177 ppm and the ^1H frequency to 4.74 ppm. The spectra were acquired with 96 t_1 increments of 512 complex points and with States-TPPI detection in the $^{13}C'$ dimension (*27*). The pulse delay was set to 1.6 s, 64 scans were added for each FID, and data accumulation was preceded by 64 dummy scans. The delays used for the longitudinal-relaxation-rate measurements were 0.01, 0.23, 0.45, 0.67, 0.89, 1.11, 1.33, and 1.55 s. The delays used for the transverse-relaxation-rate measurements were 0.004, 0.018, 0.032, 0.046, 0.060, 0.074, 0.088, and 0.102 s. All experimental data were acquired with the relaxation delays in random order. The spin-lock strength was 3 kHz.

The steady-state NOE from ^1H to $^{13}C'$ was measured with the same parameters as above except that the pulse delay

was 5.0 s in the reference experiment without NOE. This delay was substituted by a train of 998 120° ^{1}H pulses with 5 ms delays between pulses in the experiment recorded with steady-state NOE.

Longitudinal- and transverse-relaxation-rate experiments at 14.1 T were performed using the same pulse sequences as at 11.7 T but with the following differences. The spectral widths were 8000 Hz in the ^{1}H dimension and 2500 Hz in the ^{13}C′ dimension. Only 48 scans were added for each FID with 32 dummy scans before the first acquired FID. The same relaxation delay list was used for the longitudinal-relaxation-rate measurement at 14.1 and 11.7 T. Longitudinal relaxation rates were also measured using a modified pulse sequence with cross-correlation suppression, but with all other experimental parameters unchanged. For the transverse-relaxation-rate measurement, the following relaxation delays were used: 0.004, 0.028, 0.052, 0.076, 0.100, 0.124, 0.148, and 0.172 s. The spin-lock strength was set to 3.4 kHz. Transverse relaxation rates were also measured at 14.1 T using an R_2 pulse sequence with or without suppression of cross correlation. The same parameters were used as in the other experiments at 14.1 T except that the relaxation delays were 0.020, 0.040, 0.060, 0.080, 0.100, 0.121, 0.161, and 0.201 s. The delay between refocusing pulses in the CPMG pulse train was set to 600 μs.

Several experiments were repeated in order to measure the random noise relevant for error estimates.

Data Evaluation

NMR spectra were processed and evaluated using Felix version 2.3 on a Silicon Graphics work station. Felix macros and FORTRAN programs from the package ModelFree 3.1 (Drs. M. Akke and A. Palmer, Columbia University) were used for data extraction and evaluation. The spectra were processed using cosine and cosine-squared window functions, and baseline was corrected in the ^{1}H dimension. Resonance intensities were measured as peak heights.

Noise levels were obtained from repeated experiments, and random errors in measured relaxation rates were estimated using Monte Carlo simulations (*28*). The error in the steady-state NOE measurement was estimated by repeating the measurement once. The average steady-state NOE of the two measurements is presented.

RESULTS AND DISCUSSION

Introduction

The ^{13}C′ longitudinal and transverse relaxation rates for all amino acid residues in Sso7d were measured at magnetic field strengths of 11.7 and 14.1 T using the pulse sequences presented in Figs. 1A and 1B. The steady-state NOE between ^{1}H and ^{13}C′ was measured at 11.7 T using the pulse sequence presented in Fig. 1C. The relaxation rates and steady-state NOEs for Sso7d are presented as a function of amino acid residue number in Figs. 2A–2C. The average relaxation rates and steady-state NOE, not including the mobile C-terminal residues 60–63, are summarized in Table 1. A steady-state $\{^{1}H\}-^{13}C'$ NOE is observed for all amino acid residues in Sso7d, indicating the presence of sizable DD interactions between protons and ^{13}C′.

Several relaxation mechanisms need to be taken into account when analyzing ^{13}C′ relaxation in proteins enriched in both ^{13}C and ^{15}N. The most important is the chemical-shift anisotropy (CSA) relaxation mechanism. The direction-dependent chemical shift of ^{13}C′ causes relaxation in a tumbling protein. This is the dominant mechanism for ^{13}C′ relaxation (*vide infra*). Another important mechanism for ^{13}C′ relaxation is dipole–dipole (DD) relaxation. The ^{13}C′ nuclei sense the magnetic field generated by other spins in the environment, modulated by the protein motions. It is necessary to take all surrounding nuclei into account, i.e., the $^{13}C^{\alpha}$, all protons, and the backbone ^{15}N. Both auto- and, if the neighboring spins are perturbed from equilibrium, cross relaxation must be considered. Finally, also the possibility of cross correlation between relaxation mechanisms that have the same symmetry must be considered (*13, 14*). In this case, the cross correlation between CSA relaxation and DD relaxation caused by $^{13}C^{\alpha}$ is the most likely candidate, since both relaxation pathways are of reasonably large magnitude and motions of the vectors involved in the two mechanisms are likely to be correlated.

Cross Correlation between CSA and DD Relaxations

First, the cross correlation between CSA relaxation and DD relaxation (*13, 14*) is considered. Pulse sequences have previously been developed for suppression of the cross-correlation effect in ^{15}N relaxation rate measurements (*29–31*). These techniques were examined in the context of our ^{13}C′ relaxation measurements. Cross correlation is suppressed by periodically applying $^{13}C^{\alpha}$ 180° pulses during the relaxation delay in order to interchange ^{13}C′ multiplet components (*30*). The components will in this case relax with the same average relaxation rate and the cross correlation is hence effectively suppressed. The rate at which the 180° $^{13}C^{\alpha}$ pulses are applied should be faster than the decay rate of the transverse components in the case of the R_2 experiment and faster than the decay rate of longitudinal components in the case of the R_1 experiment (*30*). It is experimentally very difficult to invert the $^{13}C^{\alpha}$ without affecting the ^{13}C′. A constant number of $^{13}C^{\alpha}$ 180° pulses was therefore used. The off-resonance effect on the ^{13}C′ is in this case constant for all values of the relaxation delay, affecting all amplitudes to equal extent. In the case of both R_1 and R_2 measurements, the addition of four $^{13}C^{\alpha}$ 180° pulses during the relaxation delay made no difference to the observed relaxation rates. There is no guarantee that the cross-correlation suppression

TABLE 1
Measured Average $^{13}C'$ Relaxation Rates and the Theoretical Rates Calculated from the Average Paramters of Dynamics

	Longitudinal relaxation rate (s^{-1}) at 11.7 T	Longitudinal relaxation rate (s^{-1}) at 14.1 T	Transverse relaxation rate (s^{-1}) at 11.7 T	Transverse relaxation rate (s^{-1}) at 14.1 T	Steady state $\{^1H\}-^{13}C$ NOE at 11.7 T
Measured	0.9195	0.8423	4.4600	5.7884	1.0691
Calculated	0.9020	0.8585	4.4743	5.7605	1.0676

Note. The fitted average Lipari–Szabo (*15, 16*) parameters were the overall rotational correlation time, $\tau_m = 3.32$ ns; the internal correlation time, $\tau_e = 50$ ps; the common order parameter for CSA relaxation and DD relaxation caused by $^{13}C^\alpha$ and ^{15}N, $S^2_{backbone} = 0.88$; and the order parameter for DD relaxation caused by the virtual ^1H, $S^2_{protons} = 0.79$.

is complete since the rate with which the $^{13}C^\alpha$ 180° pulses was applied is different for each different relaxation delay. However, partial suppression of the cross-correlation effect should occur (*30*) and the complete absence of any effect suggests that any cross correlation between $^{13}C'$ CSA and $^{13}C'-^{13}C^\alpha$ DD relaxation is negligible. The R_2 rates measured with and without cross-correlation suppression were in both cases about 10% larger than the $R_{1\rho}$ rates. This difference is probably due to the technical problem of handling the $^{13}C'$ and $^{13}C^\alpha$ as separate nuclei.

A second possible explanation as to why no cross-correlation effect is observed in the present experiments is that we have only measured the initial rate of decay to determine R_1 and $R_{1\rho}$. Cross correlation does not affect the early time points unless the cross-correlation rate is large, in the same way that cross relaxation does not affect the initial rate of a selective R_1 measurement.

Interpretation of Average Relaxation and Cross-Relaxation Rates

In this section, we analyze measured relaxation rates in terms of the spectral-density function in Eq. [8]. The objective is to examine if calculated contributions from different relaxation mechanisms correspond to a physically reasonable set of parameters for the dynamics of internuclear vectors in a folded protein.

The cross-correlation effect was not considered in the evaluation since it was found to be negligible. The large number of unknown parameters and the possible variation in, e.g., CSA parameters for different $^{13}C'$ nuclei along the backbone make a residue-specific analysis too complicated at this stage. We therefore preferred to use the average longitudinal and transverse relaxation rates measured at 11.7 and 14.1 T, as well as the average steady-state $\{^1H\}-^{13}C'$ NOE, measured at 11.7 T. The relaxation rates of the mobile C-terminal residues 61–63 were not included in the average. Earlier ^{15}N relaxation studies on Sso7d show only small variations in the dynamics along the part of the protein backbone chosen for the average [(*5*) and H. Berglund *et al.*, unpublished data]. The average rates were the following: $R_1(11.7\ T) = 0.920\ s^{-1}$, $R_{1\rho}(11.7\ T) = 4.46\ s^{-1}$, $R_1(14.1\ T) = 0.842\ s^{-1}$, $R_{1\rho}(14.1\ T) = 5.79\ s^{-1}$, and the average ^1H to $^{13}C'$ NOE at 11.7 T was 1.069. These average rates were used in the fitting of relaxation rate equations that include DD auto relaxation to the $^{13}C^\alpha$, ^{15}N and a virtual ^1H as well as CSA relaxation. The distances between the $^{13}C'$ and the $^{13}C^\alpha$ and amide ^{15}N were set to 1.53 and 1.32 Å, respectively (*32*). To obtain an estimate of the effective average distance between the $^{13}C'$ and the surrounding ^1H, the distance between each $^{13}C'$ and all ^1H were calculated in the previously determined structure (*9*). For each $^{13}C'$, the average distance to a virtual ^1H was calculated by adding up the distances to all ^1H to the power of -6 and then taking this sum to the power of $-1/6$. By adding these average distances for all $^{13}C'$, excluding the C-terminal residues 61–63, and dividing by the number of $^{13}C'$, an effective $^{13}C'$ to ^1H distance of 1.69 Å is obtained for Sso7d. For CSA relaxation, we used the parameters $\delta_{Z'} = 81.8\ 10^{-6}$ and $\eta = -0.82$, calculated from the chemical-shift tensor measured by solid-state NMR on a single crystal of the dipeptide [1-^{13}C]glycyl[^{15}N]glycine (*33*).

Assuming that these physical and geometrical parameters are reasonably accurate, only parameters describing the dynamics of the protein are left. Unfortunately, each of the four relaxation pathways is associated with different vectors which, in turn, require a separate set of dynamics parameters. The number of unknowns is reduced to a single overall rotational correlation time and separate order parameters and internal correlation times for the four relaxation pathways if it is assumed that Lipari–Szabo (*15, 16*) spectral-density functions are sufficient for the description of the dynamics of all vectors. The fitting is not very sensitive to the internal correlation time and a single time constant should be adequate for all vectors. The final approximation made is that the motion can be characterized by two order parameters, one order parameter for CSA relaxation and DD relaxation caused by $^{13}C^\alpha$ and ^{15}N, and a second order parameter for $^{13}C'$ relaxation caused by the surrounding ^1H. This division was motivated because order parameters characterizing the backbone motion might be different than $^{13}C'$ to ^1H order parameters.

The fit was performed using Mathematica (*34*) to minimize the target function

$$\text{Target} = \left(\frac{R_2^{\text{exp.}}(11.7\text{ T}) - R_2^{\text{calc.}}(11.7\text{ T})}{R_2^{\text{error}}(11.7\text{ T})}\right)^2 + \left(\frac{R_2^{\text{exp.}}(14.1\text{ T}) - R_2^{\text{calc.}}(14.1\text{ T})}{R_2^{\text{error}}(14.1\text{ T})}\right)^2 + \left(\frac{R_1^{\text{exp.}}(11.7\text{ T}) - R_1^{\text{calc.}}(11.7\text{ T})}{R_1^{\text{error}}(11.7\text{ T})}\right)^2 + \left(\frac{R_1^{\text{exp.}}(14.1\text{ T}) - R_1^{\text{calc.}}(14.1\text{ T})}{R_1^{\text{error}}(14.1\text{ T})}\right)^2 + \left(\frac{\text{NOE}^{\text{exp.}}(11.7\text{ T}) - \text{NOE}^{\text{calc.}}(11.7\text{ T})}{\text{NOE}^{\text{error}}(11.7\text{ T})}\right)^2, \quad [10]$$

where exp. and calc. stand for experimental and theoretically calculated, respectively. The errors were the standard deviation for the different parameters over the residues used in the calculation of the average values. We note that R_2 in the target function, i.e., the transverse relaxation rate, actually is measured as $R_{1\rho}$, which is the rotating-frame relaxation rate. Strictly, this means that the $J(0)$ spectral density in Eqs. [2] and [4] should be replaced by $J(\omega_e)$, where ω_e is the frequency of the spin-lock field. This difference, as well as the effect of (unknown) chemical-exchange contributions to $R_{1\rho}$, was neglected.

Fitting the four unknown parameters of dynamics to the four average relaxation rates and the steady-state $\{^1\text{H}\}-^{13}\text{C}'$ NOE gave the following result: the rotational correlation time, $\tau_m = 3.32$ ns; the internal correlation time, $\tau_e = 50$ ps; the common order parameter for CSA relaxation and DD relaxation caused by $^{13}\text{C}^\alpha$ and ^{15}N, $S^2_{\text{backbone}} = 0.88$; and the order parameter for DD relaxation caused by the virtual ^1H, $S^2_{\text{protons}} = 0.79$. The average relaxation rates back-calculated from the fitted dynamics parameters are compared to average measured rates in Table 1.

The overall rotational correlation time as calculated from $^{13}\text{C}'$ relaxation data is fairly close to that measured by ^{15}N relaxation, i.e., 3.1 ns (*5*). The average order parameter for CSA relaxation and DD relaxation caused by $^{13}\text{C}^\alpha$ and ^{15}N is in the range expected for motion involving two heavier atoms (*11*). The order parameter for the $^{13}\text{C}'$ to ^1H motion is somewhat smaller than the backbone order parameter. The fitting does not change the starting value of the internal correlation time τ_e. Fitting with different starting values shows that 50 ps corresponds to a broad minimum, and the fitting does not converge well if $25 \geqslant \tau_e \geqslant 400$ ps. The balance between the two order parameters depends on the exact value of the internal correlation time.

The effects of perturbations of the input data on the fitting of the parameters of dynamics were examined. If the longitudinal relaxation rates are decreased, the target function becomes smaller. The rotational correlation time becomes longer and more different than the experimental value (*5*), while the common order parameter for the backbone vectors becomes smaller than the order parameter for ^1H relaxation. An increase of the transverse relaxation rates improves the target function but also increases the calculated rotational correlation time, whereas the two order parameters remain about the same. A reduction of the steady-state $\{^1\text{H}\}-^{13}\text{C}'$ NOE improves the target function, the order parameter for ^1H relaxation becomes larger than the order parameter for the other relaxation mechanisms, and the rotational correlation time does not change.

Given the fitted dynamics parameters, it is possible to compare how much the various relaxation mechanisms contribute to the overall relaxation of the $^{13}\text{C}'$. At 11.7 T, the relative contributions to the longitudinal relaxation are as follows: CSA relaxation, 64%; DD relaxation due to protons, 21%; DD relaxation due to $^{13}\text{C}^\alpha$, 9%; and DD relaxation due to ^{15}N, 5%. For transverse relaxation, the contributions are CSA relaxation, 73%; DD relaxation due to protons, 21%; DD relaxation due to $^{13}\text{C}^\alpha$, 4%; and DD relaxation due to ^{15}N, 2%.

The field dependence is not very large. CSA relaxation parameters found in the literature are consistent with the measured field dependence within the experimental accuracy. A large contribution to total relaxation from DD relaxation is needed in order to get a good fit of theory to experimental data since the contribution from CSA is limited by the field dependence. The contribution to total relaxation from ^1H is larger than might have been expected but the data are consistent with distances measured in the known structure. The proton relaxation contribution can be minimized by performing the experiments in D_2O while exciting and detecting via the α protons.

It can also be noted that the contribution from DD relaxation caused by the $^{13}\text{C}^\alpha$ is small. It contributes only 9 and 4% to the longitudinal relaxation and transverse relaxation rates at 11.7 T of the $^{13}\text{C}'$, respectively. A larger contribution to the longitudinal relaxation rate of the $^{13}\text{C}'$ was expected since homonuclear longitudinal relaxation includes the zero-frequency spectral density, which for a molecule in the slow-motion limit is much larger than the spectral density at other sampled frequencies. However, the distance between the $^{13}\text{C}'$ and the $^{13}\text{C}^\alpha$ is quite long and the smaller magnetogyric ratio for $^{13}\text{C}^\alpha$ compared to ^1H makes surrounding ^1H a more important source of DD relaxation for $^{13}\text{C}'$. It can noted that the relatively small size of the DD relaxation caused by the $^{13}\text{C}^\alpha$ provides an explanation to the small cross correlation between CSA and DD relaxation.

Sequence-Specific Relaxation

The longitudinal and transverse relaxation rates as a function of residue number are shown in Figs. 2A and 2B, respec-

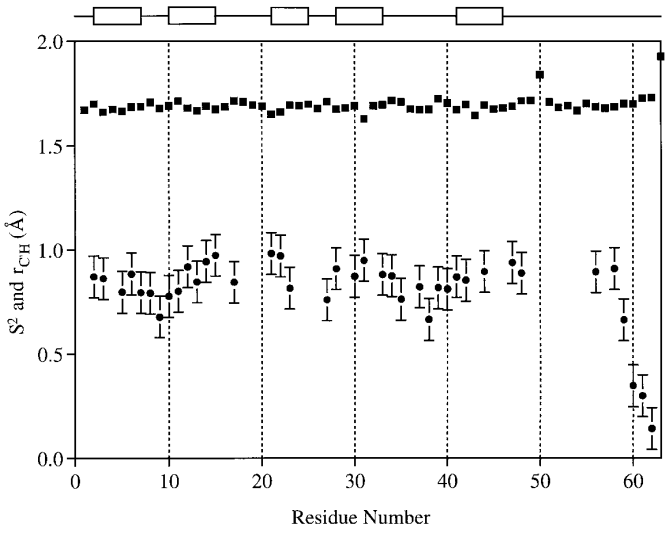

FIG. 3. The common order parameter for CSA relaxation and DD relaxation caused by $^{13}C^{\alpha}$ and ^{15}N (filled circles) and distances between each $^{13}C'$ along the backbone and the corresponding virtual proton (filled squares) as a function of residue number for the DNA-binding thermostable protein Sso7d. In the fit, only the common order parameter and the internal correlation time were allowed to change. All other parameters describing relaxation were fixed to the values obtained from the global fit as shown in Table 1. The distances between each $^{13}C'$ and all ^{1}H were calculated based on the previously determined structure (*9*). For each $^{13}C'$, the average distance to a virtual ^{1}H was calculated by adding up the distances to all ^{1}H to the power of -6 and then taking this sum to the power of $-1/6$. The error bars for the order parameters are arbitrarily set to ± 0.1. The boxes above the figure indicate β sheets present in the structure.

tively. They appear to indicate a large variation of dynamics along the backbone of the protein. The main reason for the variations observed should, in that case, be differences in the order parameter for CSA relaxation, since this is the dominating relaxation mechanism according to the analysis of average relaxation rates. A correlation between order parameters measured using ^{15}N relaxation and transverse $^{13}C'$ relaxation rates can be observed (not shown), but the variation among the transverse $^{13}C'$ relaxation rates is larger. It is not clear if these differences arise because transverse $^{13}C'$ relaxation rates are more sensitive to backbone dynamics or if they are caused by differences in the sequence-specific CSA and DD relaxation parameters.

The common order parameter for CSA relaxation and DD relaxation caused by $^{13}C^{\alpha}$ and ^{15}N as a function of residue number is shown in Fig. 3, which also shows the variation of the distances between each $^{13}C'$ along the backbone and the corresponding virtual proton. In the fit, only the common order parameter and the internal correlation time were allowed to change. All other parameters describing relaxation were fixed at the values obtained from the global fit (Table 1). The β sheets present in the structure are indicated as boxes above the figure, and they correspond to reasonably large order parameters. The larger mobility in the loop consisting of residues 8–9 and in the C-terminal fragment can be observed as smaller order parameters.

The parameters describing $^{13}C'$ CSA relaxation, $\delta_{Z'}$ and η, do not have the same values for different amino acids, and a variation is also observed even for the same amino acid, depending on the neighboring amino acid (*33, 35, 36*). The range of the principal values of the chemical-shift tensor as measured using solid-state NMR is considerable and corresponds to a variation in the CSA relaxation rate of about 10%. It has also been shown that one of the components of the chemical-shift tensor is strongly dependent on the protonation state of the carboxyl group (*37, 38*). This corresponds to a 30% more rapid CSA relaxation rate in a protonated carboxyl compared to a deprotonated carboxyl. Since the CSA relaxation rate is dependent on the protonation state, hydrogen bonding could also be expected to influence the rate. However, no such effect can be observed in the current experimental relaxation data. It is also not clear how well the chemical-shift tensors measured using solid-state NMR correspond to liquid-state relaxation data since lattice-dependent interactions have been proposed to be the source of the differences observed in the shift tensors (*35*).

The influence of ^{1}H DD relaxation has also been shown to be large and the relaxation rates for $^{13}C'$ with unusually many or few protons in the neighborhood could deviate from the average rates. On the other hand, the effective distances to the virtual protons all fell within a narrow range in Sso7d; see Fig. 3. This effect might therefore not complicate an interpretation in terms of sequence-specific dynamics as much as uncertainties in the CSA parameters.

No correlation between $^{13}C'$ relaxation rates and type of amino acid or backbone conformation was found, possibly due to the limited data set.

Possible Errors

Cross relaxation is a problem that will affect the longitudinal-relaxation-rate measurements. Cross relaxation between the $^{13}C^{\alpha}$ and the $^{13}C'$ should not be a problem using the pulse sequence shown in Fig. 1A, since the $^{13}C^{\alpha}$ is unperturbed until after the relaxation delay. From the carbon point of view, a selective carbonyl experiment has been performed and no first-order cross relaxation should occur. However, in our longitudinal-relaxation-rate pulse sequence, both ^{1}H and ^{15}N are perturbed from equilibrium at the start of the relaxation delay. No decoupling of either ^{15}N or ^{1}H is applied during the relaxation delay. Since DD auto relaxation caused by ^{1}H is important, the heteronuclear cross relaxation could possibly also be important. However, the heteronuclear ^{1}H to $^{13}C'$ cross relaxation rate is small (2%) compared to the total $^{13}C'$ longitudinal relaxation rate and should not influence the present $^{13}C'$ R_1 measurement.

The NH protons are excited and observed in these experiments. The water becomes saturated as a consequence of

the applied pulsed field gradients. Chemical exchange will transfer this saturation to the NH protons since the water will stay partially saturated between scans due to the fairly long water T_1 (*39*). However, the number of ^{1}H pulses is constant for each relaxation delay and no systematic differences between relaxation delay points should occur since the water is always identically saturated at the end of each transient.

CONCLUSIONS

The principal relaxation mechanisms for $^{13}C'$ NMR relaxation in a ^{13}C, ^{15}N-labeled protein have been examined and the use of $^{13}C'$ relaxation rates as a probe of molecular dynamics in proteins has been evaluated. $^{13}C'$ relaxation appears to be dominated by the CSA mechanism, as expected. It is shown that cross correlation between CSA and DD relaxation due to $^{13}C^{\alpha}$ is negligible. Relaxation of $^{13}C'$ caused by the surrounding ^{1}H provides a large and important contribution to the total $^{13}C'$ relaxation. DD relaxation induced by $^{13}C^{\alpha}$ and ^{15}N is also important for $^{13}C'$ relaxation, but the contributions are smaller than that due to ^{1}H. The large number of contributing relaxation mechanisms, with partially unknown physical and geometrical parameters, complicates the use of $^{13}C'$ relaxation as a sequence-specific probe for protein dynamics.

ACKNOWLEDGMENTS

This work was supported by the Swedish Natural Sciences Research Council, the Magnus Bergwall Foundation, and the Sven och Ebba-Christina Hagbergs Foundation. We thank the Swedish NMR center for time on their Varian Unity 600 MHz spectrometer.

REFERENCES

1. A. Abragam, ''Principles of Nuclear Magnetism,'' Oxford Univ. Press, Oxford, 1961.
2. N. Tjandra, S. E. Feller, R. W. Pastor, and A. Bax, *J. Am. Chem. Soc.* **117,** 12,562 (1995).
3. N. J. Skelton, A. G. Palmer III, M. Akke, J. Kördel, M. Rance, and W. J. Chazin, *J. Magn. Reson. B* **102,** 253 (1993).
4. N. A. Farrow, R. Muhandiram, A. U. Singer, S. M. Pascal, C. M. Kay, G. Gish, S. E. Shoelson, T. Pawson, J. D. Forman-Kay, and L. E. Kay, *Biochemistry* **33,** 5984 (1994).
5. H. Berglund, H. Baumann, S. Knapp, R. Ladenstein, and T. Härd, *J. Am. Chem. Soc.* **117,** 12,883 (1995).
6. T. Yamazaki, R. Muhandiram, and L. E. Kay, *J. Am. Chem. Soc.* **116,** 8266 (1994).
7. J. Engelke and H. Rüterjans, *J. Biomol. NMR* **5,** 173 (1995).
8. T. Härd, H. J. Barnes, C. Larsson, J.-Å. Gustafsson, and J. Lund, *Nature Struct. Biol.* **2,** 983 (1995).
9. H. Baumann, S. Knapp, T. Lundbäck, R. Ladenstein, and T. Härd, *Nature Struct. Biol.* **1,** 808 (1994).
10. K. T. Dayie and G. Wagner, *J. Magn. Reson. B* **109,** 105 (1995).
11. F. Cordier, B. Brutcher, and D. Marion, *J. Biomol. NMR* **7,** 163 (1996).
12. L. Zeng, M. W. F. Fischer, and E. R. P. Zuiderweg, *J. Biomol. NMR* **7,** 157 (1996).
13. M. Goldman, *J. Magn. Reson.* **60,** 437 (1984).
14. M. Guéron, J. L. Leroy, and R. H. Griffey, *J. Am. Chem. Soc.* **105,** 7262 (1983).
15. G. Lipari and A. Szabo, *J. Am. Chem. Soc.* **104,** 4546 (1982).
16. G. Lipari and A. Szabo, *J. Am. Chem. Soc.* **104,** 4559 (1982).
17. C. Dalvit and G. Bodenhausen, *Chem. Phys. Lett.* **161,** 554 (1989).
18. H. Baumann, S. Knapp, A. Karshikoff, R. Ladenstein, and T. Härd, *J. Mol. Biol.* **247,** 840 (1995).
19. S. Knapp, A. Karshikoff, K. D. Berndt, P. Christova, B. Atanasov, and R. Ladenstein, *J. Mol. Biol.* **264,** 1132 (1996).
20. D. P. Burum and R. R. Ernst, *J. Magn. Reson.* **39,** 163 (1980).
21. G. Wider and K. Wüthrich, *J. Magn. Reson. B* **102,** 239 (1993).
22. S. L. Patt, *J. Magn. Reson.* **96,** 94 (1992).
23. M. A. McCoy and L. Mueller, *J. Magn. Reson.* **99,** 18 (1992).
24. A. Bax and S. Pochapsky, *J. Magn. Reson.* **99,** 638 (1992).
25. V. Sklenář, D. Torchia, and A. Bax, *J. Magn. Reson.* **73,** 375 (1987).
26. R. Freeman and H. D. W. Hill, *J. Chem. Phys.* **54,** 3367 (1971).
27. D. Marion, M. Ikura, R. Tschudin, and A. Bax, *J. Magn. Reson.* **85,** 393 (1989).
28. A. G. Palmer III, M. Rance, and P. E. Wright, *J. Am. Chem. Soc.* **113,** 4371 (1991).
29. J. Boyd, U. Hommel, and I. D. Campbell, *Chem. Phys. Lett.* **175,** 477 (1990).
30. L. E. Kay, L. K. Nicholson, F. Delaglio, A. Bax, and D. A. Torchia, *J. Magn. Reson.* **97,** 359 (1992).
31. A. G. Palmer III, N. J. Skelton, W. J. Chazin, P. E. Wright, and M. Rance, *Mol. Phys.* **75,** 699 (1992).
32. J. K. Fawcett, N. Camerman, and A. Camerman, *Acta Crystallogr. B* **31,** 658 (1975).
33. R. E. Stark, L. W. Jelinski, D. J. Ruben, D. A. Torchia, and R. G. Griffin, *J. Magn. Reson.* **55,** 266 (1983).
34. S. Wolfram, ''Mathematica: A System for Doing Mathematics by Computer,'' Addison-Wesley, New York, 1991.
35. T. G. Oas, C. J. Hartzell, T. J. McMahon, G. P. Drobny, and F. W. Dahlquist, *J. Am. Chem. Soc.* **109,** 5956 (1987).
36. C. J. Hartzell, M. Whitfield, T. G. Oas, and G. P. Drobny, *J. Am. Chem. Soc.* **109,** 5966 (1987).
37. Z. Gu, R. Zambrano, and A. McDermott, *J. Am. Chem. Soc.* **116,** 6368 (1994).
38. N. Asakawa, S. Kuroki, H. Kurosu, I. Ando, A. Shoji, and T. Ozaki, *J. Am. Chem. Soc.* **114,** 3261 (1992).
39. S. Grzesiek and A. Bax, *J. Am. Chem. Soc.* **115,** 12,593 (1993).